J Appl Electrochem (2008) 38:551–560
DOI 10.1007/s10800-007-9472-4

ORIGINAL PAPER

Time averaged temperature calculations in pulse electrochemical machining, part II: numerical simulation

N. Smets · S. Van Damme · D. De Wilde · G. Weyns · J. Deconinck

Received: 27 April 2007 / Revised: 12 December 2007 / Accepted: 13 December 2007 / Published online: 3 January 2008

Abstract Simulation of the temperature distribution and evolution during pulse electrochemical machining can be a computationally very expensive procedure. In a previous part of the work [Smets et al. *J Appl Electrochem* 37(11):1345, 2007] a new approach to calculate the temperature evolution was introduced: the hybrid method, which combines averaged and pulsed calculations. The averaged calculations are performed by time averaging the boundary conditions and the bulk heat sources of the system. The timesteps used during the averaged calculations are then no longer dictated by the pulse characteristics. Using this approach, computationally very cheap, yet satisfactory results can be obtained. The analysis in the previous part of the work was obtained from analytical solutions on simplified models. In this part, the more general case is solved numerically. Multiple geometries are simulated and analyzed and methods are compared. Very satisfactory, yet cheap results are obtained.

Keywords Pulse electrochemical machining · Simulations · Temperature distribution · Time averaging · Transient · FEM

List of symbols

a	Polarization parameter 1, S m^{-2}
A	Electrode surface, m^2
b	Polarization parameter 2, A m^{-2}
Bi	Biot number
C_p	Heat capacity, J kg^{-1} K^{-1}
$D_{0,i}$	Diffusion coefficients at infinite dilution, m^2 s^{-1}
E_0	Equilibrium potential, V
F_0	Fourier number
h	Heat transfer coefficient, W m^{-2} K^{-1}
H	Characteristic size electrode, m
I	Electrical current, A
J	Current density distribution, A m^{-2}
k	Thermal conductivity, W m^{-1} K^{-1}
L	Electrode length, m
P_{dl}	Heat produced in the double layer, W m^{-2}
P_{bulk}	Heat produced in the bulk, W m^{-3}
Pr_t	Turbulent Prandtl number
$\dot{q}$	Heat flux density, W m^{-2}
$\overline{r}$	General location vector, m
St	Strouhal number
t	Time, s
T	Pulse period, s
Δt_c	Convection time scale, s
U	Potential distribution, V
v	Scalar velocity, m s^{-1}
$\overline{v}$	Velocity vector, m s^{-1}
x	Distance, m

Greek symbols

α	Duty cycle
α'	Thermal diffusivity, m^2 s^{-1}
η	Overpotential, V
θ	Relative temperature, K
θ'	Normalized temperature, K
$\overline{\theta}$	Averaged temperature, K
$\tilde{\theta}$	Temperature ripple, K
θ_{decay}	Decaying temperature, K
Θ	Temperature, K
Θ_i	Initial temperature, K
Θ_∞	Reference temperature, K
Θ^*	Steady state temperature, K

N. Smets (✉) · S. Van Damme · D. De Wilde · G. Weyns · J. Deconinck
Vrije Universiteit Brussel IR/ETEC, Pleinlaan 2, 1050 Brussels, Belgium
e-mail: nsmets@vub.ac.be

$\hat{\lambda}_n$	Transcendental coefficients
μ	Dynamic viscosity, kg m^{-1} s^{-1}
ρ	Density, kg m^{-3}
σ	Electrical conductivity, S m^{-1}
τ	Time constant, s
ψ	Pulse delay, s

Abbreviations

2D	Two dimensional
BC	Boundary condition
ECM	Electrochemical machining
FEM	Finite elements method
FTAS	Full time accurate simulation
PECM	Pulse electrochemical machining
QSS	Quasi steady state
QSSSC	Quasi steady state shortcut
RANS	Reynolds averaged Navier–Stokes
SS	Steady state

1 Introduction

Electrochemical machining (ECM) is a manufacturing process based on the controlled anodic dissolution of a metal at large current densities (in the range of 1 A mm^{-2}). An electrolytic cell is created in which the tool (cathode) is advanced towards the work-piece (anode). The electrolyte is pumped through the electrode gap at high speed to carry away reaction products, heat and gas.

When it comes to the machining of components of complex geometry and hard material, ECM has obvious advantages over conventional milling or turning procedures: it can be applied regardless of material hardness, there is no tool wear and a high quality surface can be obtained with no residual stresses or damage to the microstructure [1–3]. Many high quality parts are prepared by ECM, from shaver heads to turbine blades.

Despite its advantages, some difficulties still trouble the application of ECM. One important issue is the lack of quantitative simulation software to predict the tool shape and machining parameters necessary to produce a given work-piece profile [3–5]. The most complete model needs to deal with the effects of the fluid flow, gas evolution, heat generation, the electrochemical processes at the electrodes, the transport of the species involved and all this while the electrode shape changes. This work makes a contribution in incorporating the heat generation in the model, and calculating the temperature distributions. The gas evolution and shape change are not yet incorporated.

Pulse electrochemical machining (PECM) involves the application of current or voltage pulses. In this work only current pulses will be considered. This does not compromise the generality, since voltage and current are closely related. Pulsed current may be applied for reasons of accuracy and surface quality [3, 6–8]. The application of pulsed current can also reduce the thermal load on the work-piece, while still maintaining the desired current density during the pulse on-time. The issue of heating of the electrolyte is of primary importance for the determination of the limit conditions in ECM [6, 7, 9–11].

Steady state (SS) temperature distribution calculations have been performed by Kozak et al. [9], Clark and McGeough [10] and Loutrel and Cook [11]. Time accurate calculations of the temperature distribution during PECM have already been performed by Kozak [7, 8]. In [7, 8] the pulses are considered to be independent of each other, and thus no accumulation of heat over multiple periods is encountered. Cases where there was accumulation of heat in the system during multiple pulses, have been performed in former work of the author [12].

To simulate electrochemical processes with current pulses, one has to perform calculations with boundary conditions (BC's) that vary in time. All the variable distributions have to be calculated in time. The applied pulses have to be described on a time scale that can be orders of magnitude smaller than the time scale on which the thermal effects evolve. This means that one would have to calculate a lot of timesteps to perform a satisfactory thermal simulation, which would be a computationally very expensive procedure. The aim of this paper is to find a cheaper approach which would still provide satisfactory results.

By averaging the heat production in the system, it is possible to calculate temperature changes with timesteps that are not dictated by the time scale of the pulses. It also provides the possibility of calculating a SS. Plain averaging is however inadequate in the system under consideration, because of the very broad spectrum of possible time scales present (see also [12]). While averaging might be necessary to handle the largest time scales, the smaller time scale effects may still be very important to perform accurate simulations. The hybrid method, and more in particular the derived quasi steady state shortcut (QSSSC) were introduced [13] as a solution to this problem. The latter consists of using the averaged SS as a starting state, and applying pulses afterwards. It was shown that delaying the start of the pulse in time with a certain value ψ, influences the speed with which the quasi steady state (QSS) is reached starting from the SS. Analytical formulae for optimal values ψ of were presented in the work. All the theoretical findings from [13] are put into practice in this part of the work for detailed numerical simulations, using the Finite Element Method.

2 Mathematical model

This paper concentrates on thermal aspects. The full electrochemical model used in this work is described in a separate paper [14].

In order to find the local flow field the incompressible Reynolds averaged Navier–Stokes (RANS) equations are solved. The turbulent viscosity which enters these equations, is calculated using the low-*Re* k-ω turbulence model. A detailed description of the equations, the BC's and the numerical solution techniques can be found in [15].

The excess supporting electrolyte ensures that the potential distribution U in the electrolyte is governed by the Laplace equation

$$\overline{\nabla} \cdot \left(\sigma \overline{\nabla} U\right) = 0 \tag{1}$$

with non-linear BC's due to the electrochemical reactions. The electrical conductivity σ, is a function of the temperature Θ and a function of ionic concentrations, of which the latter is extensively treated in [14]. The diffusion coefficients at infinite dilution $D_{0,i}$, used to calculate the conductivity [14], are increased 2% per Kelvin [16].

The local current density J can be calculated using

$$\overline{J} = -\sigma \overline{\nabla} U. \tag{2}$$

A linearized overpotential is used to model the polarization on the surface of the electrodes,

$$J = a\eta + b, \tag{3}$$

where the equilibrium potential E_0 is deliberately assumed to be zero, which does not compromise the generality.

The current efficiency on the anode, where the electrochemical dissolution of the metal takes place, is assumed to be 100%, so no current is consumed by the production of oxygen gas.

In this system (also in [14]), metal ions Fe^{2+}, Fe^{3+} and Cr^{6+} at the anode and hydroxide ions OH^- at the cathode strongly influence the local conductivity σ. Ion production at the electrodes is calculated from the local current density. The ion distributions are calculated using convection–diffusion equations with mass fluxes on the boundaries [14].

The temperature distribution in the system is calculated using a convection–diffusion equation with heat sources,

$$\rho C_p \frac{\partial \Theta}{\partial t} + \rho C_p \overline{v} \cdot \overline{\nabla} \Theta = \overline{\nabla} \cdot \left(k \overline{\nabla} \Theta\right) + P_{\text{bulk}}. \tag{4}$$

The thermal conductivity k is composed of the molecular k_{mol} thermal conductivity and the turbulent thermal conductivity k_{turb} [17],

$$k = k_{\text{mol}} + k_{\text{turb}}. \tag{5}$$

Joule heating in the bulk of both the electrolyte and the electrodes is considered, where

$$P_{\text{bulk}} = \frac{J^2}{\sigma}. \tag{6}$$

Heat dissipation in the double layer, where [11]

$$P_{\text{dl}} = \eta J, \tag{7}$$

is also taken into account. P_{dl} is imposed as heat flux at the electrode surfaces that are the boundaries of two domains: the electrodes and the electrolyte. The boundaries of the electrodes, which are not contiguous to the electrolyte, are considered thermal insulators. This choice is justified by the fact that essentially all of the heat generated in the system must be carried away by the electrolyte [11].

All partial differential equations presented above were solved in two spatial dimensions (2D) using the residual distribution method [18]. The scalar N-scheme was applied to the convective terms in the convection–diffusion equations. Equal distribution was applied to the diffusion terms. All numerical schemes provided at least second order accuracy [19]. An implicit second order—time accurate—time integration scheme was used [20, 21].

3 Time averaging

3.1 Averaging the current

A current pulse is characterized by the duty cycle α, the period T, and the value of the current during the on-time of the pulse I_{on}, see Fig. 1a. The duty cycle α is the ratio of the pulse on-time to the total period T of the pulse. The total current I is applied to the system, resulting in a local current density distribution J such that

$$I(t) = \int_A J(\overline{r}, t) dA \tag{8}$$

with A a surface through which the current I flows. All the current I is considered to be faradaic. Averaging the total current gives,

$$I_{\text{av}} = \alpha I_{\text{on}}. \tag{9}$$

Using Eqs. 8 and 9, give for the local current densities

$$\int_A J_{\text{av}}(\overline{r}) dA = \alpha \int_A J_{\text{on}}(\overline{r}) dA. \tag{10}$$

The shape of the current density profiles is dependent of the magnitude of the applied current. However, very often the shapes of the current density profiles tend to each other (e.g. edge effects), and one can say that in approximation

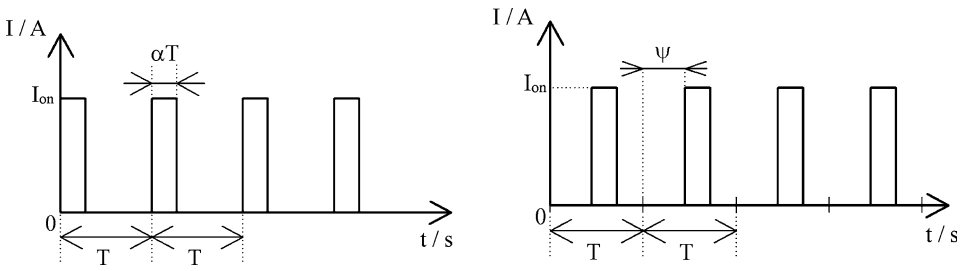

Fig. 1 Applied current pulses, with period T, duty cycle α and amplitude I_{on}. (**a**) Immediate on-time; (**b**) Delaying the pulses in time with ψ

$$J_{av}(\overline{r}) \approx \alpha J_{on}(\overline{r}) \tag{11}$$

3.2 Averaging the heat production

The heat production also needs to be averaged. If the average current is applied, then the average heat will not be produced, because of the non-linear relationships. The heat sources in the equations are to be adapted in such a way that the average heat production is obtained.

3.2.1 Heat production in the double layers

Neglecting endo- or exothermal effects, the heat production in the double layer is

$$P_{dl}(\overline{r},t) = \eta(\overline{r},t)J(\overline{r},t). \tag{12}$$

The averaged heat production in the double layer during a period T is

$$P_{av,dl}(\overline{r}) = \alpha\eta_{on}(\overline{r})J_{on}(\overline{r}). \tag{13}$$

For a linearized overpotential (Eq. 3), and considering Eqs. 11, 13 yield

$$P_{av,dl}(\overline{r}) \approx \left(\frac{J_{av}(\overline{r})}{a\alpha} - \frac{b}{a}\right)J_{av}(\overline{r}) \tag{14}$$

Equation 14 provides the local averaged heat production $P_{av,dl}$ in the double layer, as a function of the local averaged current density J_{av}.

If a more complex polarization behaviour is considered, for example a Butler–Volmer polarization, analogous, yet more complex, equations for $P_{av,dl}$ are obtained.

3.2.2 Heat production in the bulk

In both the electrolyte and the electrodes there is heat generation (Joule effect). For the dissipated heat

$$P_{bulk}(\overline{r},t) = -\overline{J}(\overline{r},t)\cdot\overline{\nabla}U(\overline{r},t). \tag{15}$$

Equations 2 and 15 yield

$$P_{bulk}(\overline{r},t) = \sigma\left(\overline{\nabla}U(\overline{r},t)\right)^2 \tag{16}$$

Averaging this heat production over a period T gives

$$P_{av,bulk}(\overline{r}) = \alpha\sigma\left(\overline{\nabla}U_{on}(\overline{r})\right)^2. \tag{17}$$

If Eq. 11 is valid, using Eq. 2, gives for the bulk $\overline{\nabla}U_{av}(\overline{r}) \approx \alpha\overline{\nabla}U_{on}(\overline{r})$, and

$$P_{av,bulk}(\overline{r}) = \frac{\sigma}{\alpha}\left(\overline{\nabla}U_{av}(\overline{r})\right)^2. \tag{18}$$

Equation 18 provides the local averaged heat production $P_{av,bulk}$ in the bulk, as a function of the local averaged potential distribution U_{av}.

4 Theoretical basis

The main findings of former work [12] and [13], which are of importance here, are briefly noted for use in the following sections.

First the relative temperature is defined as

$$\theta = \Theta - \Theta_{\infty}, \tag{19}$$

with Θ_{∞} the electrolyte temperature.

In the electrode the $\theta(x, t)$ temperature evolution can be decomposed into the average temperature $\overline{\theta}(x,t)$, the ripple $\tilde{\theta}(x,t)$ (with an average of zero) and the decaying component $\theta_{decay}(x, t)$,

$$\theta(x,t) = \overline{\theta}(x,t) + \tilde{\theta}(x,t) + \theta_{decay}(x,t). \tag{20}$$

The undesirable $\theta_{decay}(x, t)$ can be reduced by delaying the pulses with a time interval ψ. The optimal value $\psi = \psi^*$ is analytically obtained on a simplified model,

$$\psi^* = \tau_1 \ln\left(\alpha\frac{e^{T/\tau_1}-1}{e^{\alpha T/\tau_1}-1}\right). \tag{21}$$

The largest time constant τ_1 for the conduction in the electrode is

$$\tau_1 = \frac{H^2}{\alpha'\hat{\lambda}_1^2}, \tag{22}$$

where $\hat{\lambda}_1$ is the first root of the transcendental equation

$$\cot \hat{\lambda}_n = \frac{\hat{\lambda}_n}{Bi}, \tag{23}$$

where

$$Bi = \frac{hH}{k}. \tag{24}$$

The hybrid method consists of combining the averaged boundary conditions and pulses in one calculation. Starting from $t = 0$, the averaged heat sources are applied, and after time $t = t^*$, pulses are applied (possibly delayed by ψ). The temperature evolution is then

$$\theta_{\text{hybrid}}(x,t) = \overline{\theta}(x,t) + \tilde{\theta}(x,t-t^*) + \theta_{\text{decay}}(x,t-t^*), \tag{25}$$

where $\tilde{\theta}(x,t-t^*)$ and $\theta_{\text{decay}}(x,\ t-t^*)$ start from the time $t = t^*$. A particularly interesting case, is when $t^* \to \infty$. The starting state $t = t^*$ at is then the averaged SS. This situation is called the QSSSC. When performing the QSSSC, it is convenient to start the pulsed calculation from $t = 0$, while applying the averaged SS as initial state.

$$\theta_{\text{QSSSC}}(x,t) = \theta^*_{\text{av}}(x) + \tilde{\theta}(x,t) + \theta_{\text{decay}}(x,t). \tag{26}$$

It was shown in [13] that when $\psi = \psi^*$ is applied during the QSSSC, $\theta_{\text{decay}}(x,\ t)$ becomes small enough to be neglected during the on-times of the pulses for the simplified model.

The thermal dynamics of the electrode have a strong impact on the temperature evolution in the thermal boundary layer and are hence very important.

The convection time scale was found to be

$$\Delta t_c = \frac{L}{v}. \tag{27}$$

5 Numerical simulations: results and discussion

The following general data were used in the calculations. For the calculation of the flow field, the dynamic viscosity was $\mu = 0.001$ kg m^{-1} s^{-1}, the electrolyte density was $\rho_{\text{electrolyte}} = 1000$ kg m^{-3} and the average flow velocity was $v_{\text{av}} = 15$ m s^{-1}. The flow was fully developed at the channel inlet. The linearized overpotentials for the anode and the cathode were respectively

$$J_{\text{anode}} = 0.33 \times 10^6 \ \text{S m}^{-2}\eta - 0.76 \times 10^6 \ \text{A m}^{-2} \tag{28}$$

and

$$J_{\text{cathode}} = 10 \times 10^6 \ \text{S m}^{-2}\eta + 10 \times 10^6 \ \text{A m}^{-2}. \tag{29}$$

These polarization values were taken from the work of Van Damme et al. [14], who obtained the experimental data from [22]. The equilibrium potential E_0 was however not included in the measurements and is, by default, set equal to zero. This does not compromise the general principles shown in this work. The physical parameters used in the simulation for the electrolyte and electrodes can be found in Table 1. The electrolyte temperature was $\Theta_\infty = 20\,^\circ\text{C} = 293.15$ K at the inlet. For the turbulent Prandtl number the typical value $Pr_t = 0.71$ was taken [17]. The duty cycle was $\alpha = 10\%$ for all the simulations.

Table 1 Physical parameters of the electrodes and electrolyte

	Electrolyte	Electrodes
σ	16.485 S m^{-1}	1×10^6S m^{-1}
ρC_p	4.17×10^6 J m^{-3} K^{-1}	3.55×10^6 J m^{-3} K^{-1}
k	0.5984 W m^{-1} K^{-1}	81 W m^{-1} K^{-1}

All the simulations were performed on simple channels with rectangular electrodes. The meshes assured grid convergence and the smallest mesh elements in the flow channel on the electrode surfaces were 10^{-7} m in height in order to capture the thermal boundary layer in detail.

5.1 Geometry 1

The first geometry on which simulations were performed is shown in Fig. 2. The cathode was at the top, the anode was at the bottom. In the middle is the channel through which the electrolyte was pumped from left to right. The channel was 200 μm in height, yielding a Reynolds number of 3000, and hence the flow was considered turbulent. The length of the electrodes was 3 mm, the height was 0.5 mm, the depth was 10 mm (along the Z dimension). The surface of the electrodes was $A = 30$ mm^2. The applied current was $I_{\text{on}} = 30$ A during the on-time of the pulse, so that the average current density during the on-time was $J_{\text{on}} = 1$ A mm^{-2}. The pulse period was $T = 15$ ms. The geometry

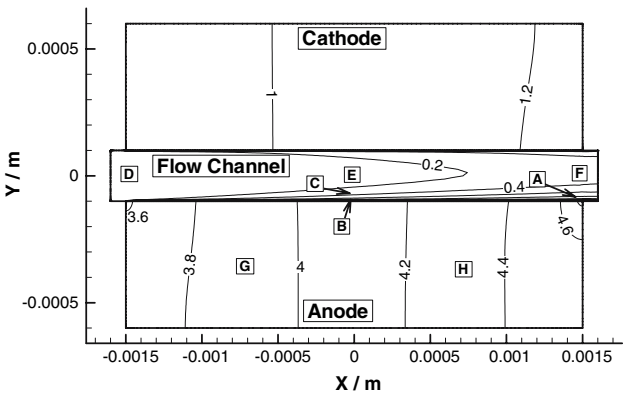

Fig. 2 Geometry 1, with 8 reference points A, B, C, D, E, F, G, and H. Also showing the averaged SS temperature distribution in 2D

was discretized in 57,962 triangular elements and 29,814 nodal points.

The calculated temperature fields were 2D and functions of time. This provided too much information to display in this paper, hence the temperature was taken from eight reference points A, B, C and D, E, F and G, H (see Fig. 2) and plotted as a function of time. A was located at the end of the anode (downstream), B in the middle of the anode, and C in the middle at a distance of 2.4 μm from the anode. Three other reference points D, E and F were located in the center of the flow channel, respectively at the start, the middle and the end of the electrodes. Two more reference points G and H are located in the anode, as shown in Fig. 2.

5.1.1 Averaged calculations

One can easily calculate I_{av}, using Eq. 9. By applying I_{av} as BC, $U_{\mathrm{av}}(\overline{r},t)$ and $J_{\mathrm{av}}(\overline{r},t)$ can be calculated. Then the averaged heat production can be calculated (Eqs. 14 and 18), from which $\overline{\theta}(\overline{r},t)$ can be calculated.

The SS temperature distribution is given in Fig. 2. Generally the local heat transfer coefficient can be calculated using

$$h(\overline{r},t)=\frac{\dot{q}(\overline{r},t)}{\theta(\overline{r},t)}. \tag{30}$$

Averaging in space yields $h(t)=\frac{1}{A}\int_A h(\overline{r},t)dA$. This averaged $h(t)$ can be further averaged in time over an interval Δt, using $h_{\mathrm{av}}=\frac{1}{\Delta t}\int_{\Delta t} h(t)dt$. In this SS case the numerical calculations yield $h_{\mathrm{av}}=130$ kW m^{-2} K^{-1} and $Bi=0.8$ and thus $\tau_1=17.5$ ms, making the conduction time scale $5\tau_1=68$ ms. The convection time scale is calculated $\Delta t_c=0.2$ ms.

When applying the averaged heat production, the averaged temperature evolution can be calculated. These are shown in Fig. 3 for the sample points. An analysis of the temperature evolution in reference points A, B, C, G and H shows that the time constant from the best fit in Fig. 3 is $\tau_1=16.7$ ms, which is very close to the value obtained above. For reference points D, E and F the much smaller convection time scale Δt_c determines the temperature evolution, and hence the temperature evolution appears to be instantaneous in Fig. 3.

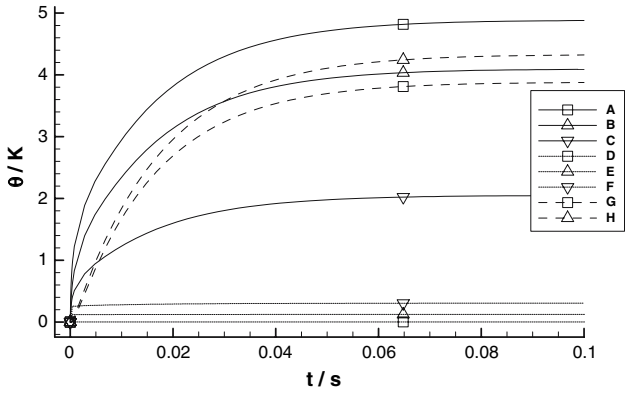

Fig. 3 Averaged temperature evolutions $\overline{\theta}$ in the sample points as a function of time

5.1.2 Full time accurate simulation

The straight forward FTAS can be performed by applying all pulses. The temperature changes for reference points A, B and C are shown in Fig. 4. The temperature changes at reference points D, E and F are quasi instantaneous because of the small Δt_c. They switch from the local SS to the next SS, see [12].

The temperature evolution can be decomposed (see Eq. 20). For example for reference point A the components are shown in Fig. 5. The averaged temperature evolution $\overline{\theta}$ is taken from Fig. 3. The ripple $\tilde{\theta}$ is determined from the QSS, by subtracting the mean value from a period. The

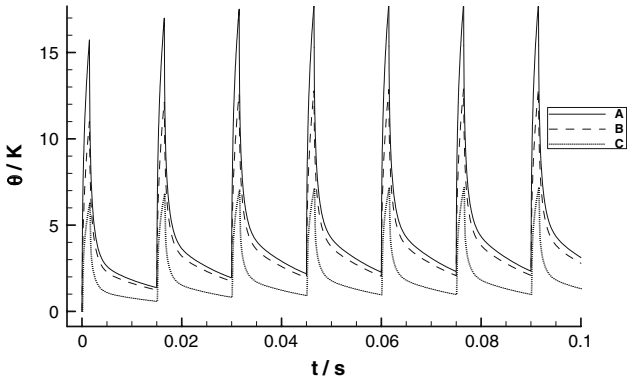

Fig. 4 Temperature evolutions θ in sample points A, B and C during FTAS

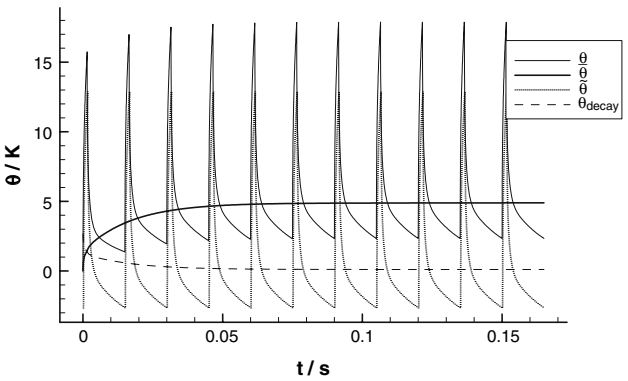

Fig. 5 Decomposition of the temperature evolution θ in $\overline{\theta}$, $\tilde{\theta}$ and θ_{decay}, for reference point A

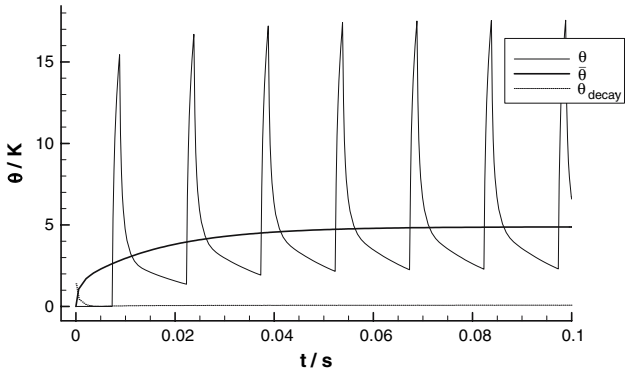

Fig. 6 Temperature evolution θ during FTAS in reference point A, pulses delayed in time with $\psi = 7.30$ ms

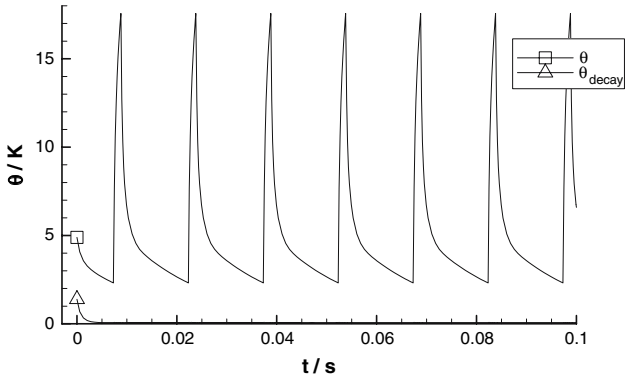

Fig. 8 Temperature evolution θ in sample point A with $\psi = 7.30$ ms, during QSSSC

decaying component is then determined as $\theta_{\text{decay}}(x,t) = \theta(x,t) - \overline{\theta}(x,t) - \tilde{\theta}(x,t)$.The term $\theta_{\text{decay}}(x,\ t)$ can also contain a constant component during the numerical calculations. In this case the averaged SS temperature is not exactly equal to the average of the QSS

If the current pulses are delayed in time (see Fig. 1b) the decaying component θ_{decay} can be minimized. The optimal delay for the conduction is chosen, since for the convection there is no accumulation spanning multiple pulses. Equation 21 yields $\psi = \psi^* = 7.30$ ms. The new temperature evolution in sample point A is shown in Fig. 6. Decomposition of the temperature evolution reveals that the decaying component has diminished significantly and rapidly becomes very small (see Fig. 6).

5.1.3 Quasi steady state shortcut (QSSSC)

Here the averaged SS is used as an initial state before applying current pulses. By applying pulses that start immediately at the beginning of the period ($\psi = 0$ s), the temperature evolution at reference point A from Fig. 7 is obtained. A decaying component can be observed in the evolution. By delaying the pulses in time with $\psi = 7.30$ ms, the decaying component is reduced significantly (see Fig. 8). The QSS is reached almost immediately and hence with a minimum of time and computational effort. The same conclusions can be drawn for the other sample points.

5.2 Geometry 2

The second geometry on which calculations were performed is shown in Fig. 9. A zoom of the flow channel is shown in Fig. 10. The averaged SS temperature distribution and the location of reference points A, B, C, D, E, F, G and H can also be seen in Figs. 9 and 10. The cathode was at the top, the anode was at the bottom. In the middle was the channel through which the electrolyte was pumped from left to right. The channel was 200 μm in height, yielding a Reynolds number of 3000, and hence the flow was considered turbulent. The length of the anode was 100 mm, the height was 50 mm and the depth was 100 mm (along the Z dimension). The length of the cathode was 80 mm and it was placed central with respect to the anode,

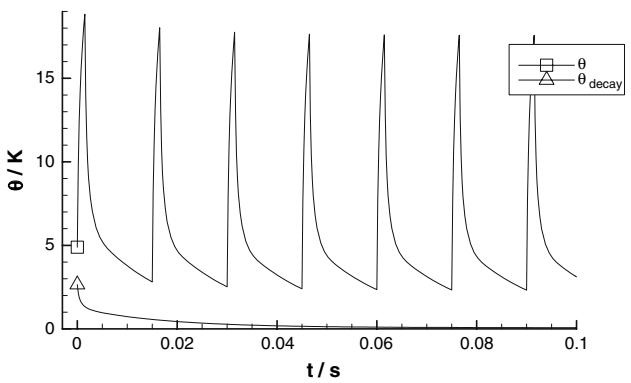

Fig. 7 Temperature evolution θ in sample point A with $\psi = 0$ s, during QSSSC

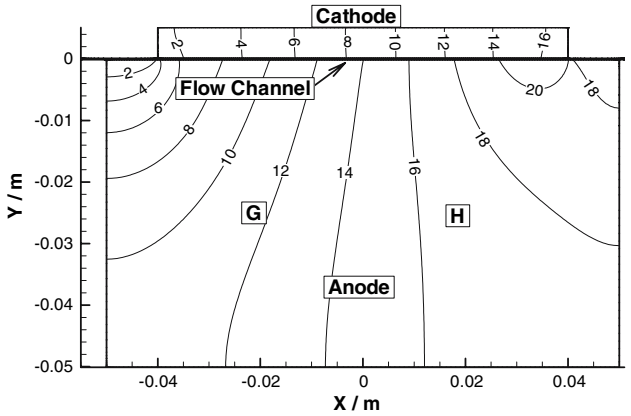

Fig. 9 Geometry 2, showing the averaged SS temperature distribution $\overline{\theta}$, and reference points G and H

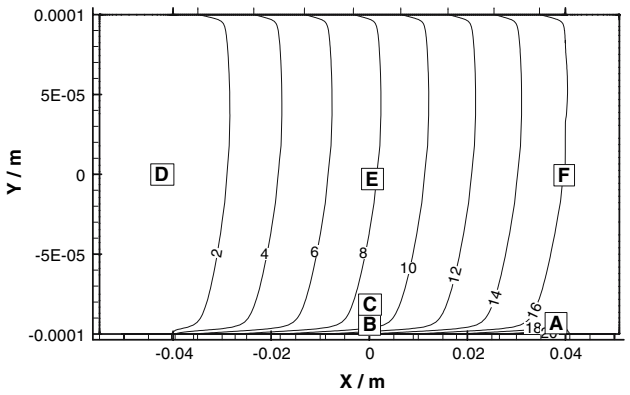

Fig. 10 Geometry 2, zoom of the channel. Showing the averaged SS temperature distribution, and reference points A, B, C, D, E and F

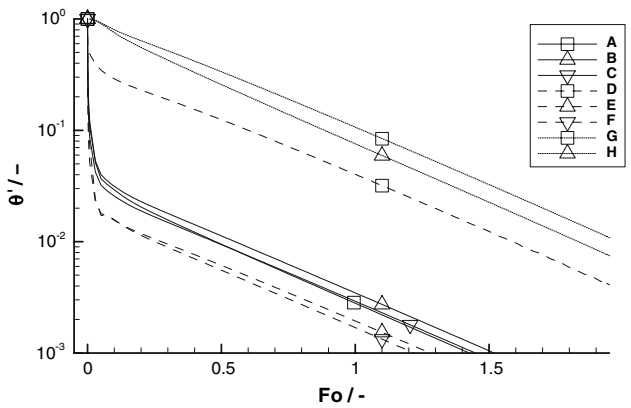

Fig. 12 Normalized temperature evolutions θ' in the sample points as a function of Fo

the height was 5 mm and the depth was 100 mm. The surface of the cathode was $A = 8000$ mm^2. The applied current was $I_{on} = 8000$ A during the on-time of the pulse, so that the average current density during the on-time was $J_{on} = 1$ A mm^{-2}. The pulse period was $T = 100$ ms. The whole mesh contained 80,532 triangular elements, and 41,266 nodal points.

5.2.1 Averaged calculations

Applying the time averaged boundary conditions and heat sources, the SS was calculated, and gave $h_{av} = 6.22$ kW m^{-2} K^{-1}. This yields a Biot number $Bi = 81$, and hence $\tau_1 = 47$ s. The conduction time scale is hence $5\tau_1 = 235$ s. The convection time scale is $\Delta t_c = 5.3$ ms. Comparing the pulse period $T = 100$ ms to Δt_c and $5\tau_1$ leads to the conclusion that $\Delta T_c < T \ll 5\tau_1$. No accumulation of heat occurs in the flow channel, but accumulation of heat does occur in the electrode and the thermal boundary layer (see also [12]).

The averaged temperature changes at the sample points are shown in Fig. 11. The temperature changes at the reference points in the channel evolve very strongly at the start, because they are located near the heating region and since the Biot number is high, the heat is not transported away easily. The normalized temperature $\theta' = \frac{\Theta - \Theta_\infty}{\Theta_i - \Theta_\infty}$ as a function of $F_0 = \frac{\alpha' t}{H^2}$ is shown in Fig. 12. For $F_0 < 0.2$, the temperature change at the reference points in the channel is controlled by much smaller time constants than τ_1. Analysis shows, that for $F_0 > 0.2$ the time constant from the best fit in Fig. 11 is $\tau_1 = 45$ s, which is very close to the value obtained above. The reference points D, E and F are also controlled by the electrode time constants because the thermal boundary layer fills the whole channel.

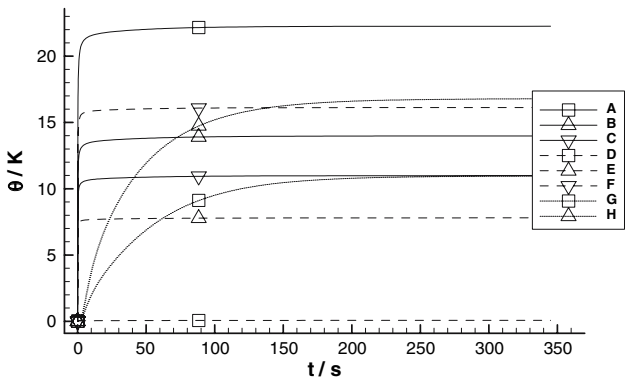

Fig. 11 Averaged temperature evolutions $\overline{\theta}$ in the sample points

5.2.2 Full time accurate simulation

A FTAS was performed on the current geometry. The pulses were delayed with $\psi = \psi^* = 45$ ms. The physical time calculated was only 3 s. A simulation up to the QSS (350 s) would have taken about 20 days to perform (On a 64 bit machine with quad CPU @ 2.66 GHz, 4 GB of RAM. Using the software package PARDISO [23, 24].). This is a good example where the FTAS would be computationally too expensive, and even practically impossible. The temperature change θ at reference point A during the first 3 s is shown in Fig. 13, together with the averaged temperature change $\overline{\theta}$. Decomposition reveals that θ_{decay} rapidly becomes very small. The same conclusion can be drawn for the other reference points.

5.2.3 Quasi steady state shortcut (QSSSC)

On this geometry, a QSSSC was applied, where the pulses were delayed with $\psi = 45$ ms. The temperature changes in Fig. 14 were obtained. Because of the choice of ψ the decaying component θ_{decay} is small, and the QSS is almost

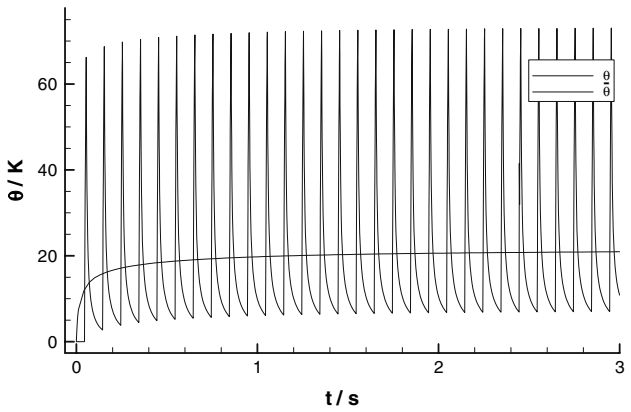

Fig. 13 Temperature evolutions, averaged and pulsed case, with $\psi = 45$ ms

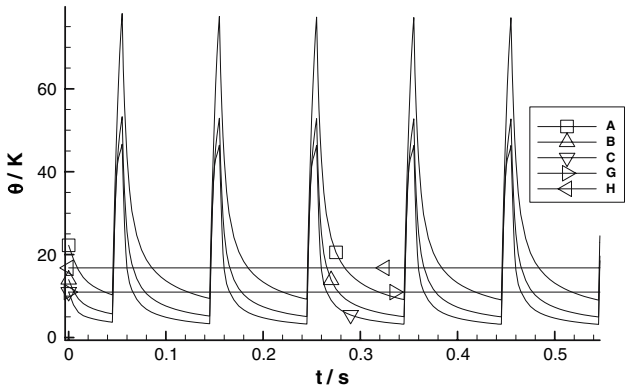

Fig. 14 Temperature evolutions during QSSSC, with $\psi = 45$ ms

immediately reached. Despite the slowest time constant τ_1 of the system being huge, there is still quite a ripple present during the QSS. This ripple is limited in space to the flow channel and the part of the electrode near the double layer heating.

This is a good example of the averaging being necessary to tackle the very large time constant τ_1, but the plain averaging being inadequate because the smaller time constants in the system give rise to a significant ripple $\tilde{\theta}$ in important locations. The QSSSC is an adequate solution to this problem.

The more pulses are calculated, the better the true QSS is approached. The decaying component θ_{decay} damps out with the same large time constant τ_1 as the whole system evolves, and hence it is valuable to be able to eliminate the slowest component by applying $\psi = \psi^*$ [13].

The first period of the QSSSC should provide satisfactory results. In that case it is not necessary to calculate the whole period, just the ψ^* off-time part, and the αT on-time part. The rest of the period is of no importance.

6 Discussion of the practical method

If the duration of the thermal transients in the system (conduction and convection) can be neglected compared to the total machining time, it is an acceptable approximation to say that the system is always in QSS. If the temperature evolution near the electrode surface is as in Fig. 11, e.g. approaching a step function, this simplification is even more acceptable. The QSS can be computed cheaply using the QSSSC. This method is convenient for easy integration in a larger time scale time stepping calculation, for instance for the calculation of the shape change of the electrodes.

If the duration of some of the thermal transients in the system (conduction or convection) cannot be neglected compared to the total machining time, it is still possible to use the hybrid method. This method is a little more expensive than the QSSSC because the averaged change has to be calculated using some large timesteps, but it is still a computationally very cheap method.

7 Conclusions

When solving thermal problems during pulsed electrochemical machining (PECM) in real systems numerical techniques are applied. As a general method to solve the thermal problem during PECM, the full time accurate simulation (FTAS) is always an option. This method can however be computationally very expensive, if not practically impossible, if the full detail of the pulses has to be considered.

If the FTAS method would be too expensive, the approximative hybrid method and the quasi steady state shortcut (QSSSC) can be used. The approximative methods perform very well for the numerical cases treated in this work. The optimal pulse delay is obtained analytically for simplified problems in former work, but applies very well for the more complex cases in this work.

References

1. Risco D, Davydov A (1993) J Am Soc Mech Eng 64:701
2. McGeough J (1974) Principles of electrochemical machining. Chapman and Hall, London
3. Rajurkar KP, Zhu D, McGeough JA, Kozak J, De Silva A (1999) Ann CIRP 48(2):567
4. Lohrengel M, Klueppel I, Rosenkranz C, Betterman H, Schultze J (2003) Electrochim Acta 48(20–22):3203
5. Mount A, Clifton D, Howarth P, Sherlock A (2003) J Mater Process Technol 138:449
6. Datta M, Landolt D (1981) Electrochim Acta 26(7):899
7. Kozak J (2004) Bull Polish Acad Sci Tech Sci 52(4):313
8. Kozak J, Rajurkar K (1991) J Mater Process Technol 28(1–2):149

9. Kozak J, Rajurkar K, Lubkowski K (1997) Trans NAMRI/SME XXV:159
10. Clark W, McGeough J (1977) J Appl Electrochem 7:277
11. Loutrel S, Cook N (1973) ASME J Eng Ind 95(B/4):1003
12. Smets N, Van Damme S, De Wilde D, Weyns G, Deconinck J (2007) J Appl Electrochem 37(3):315
13. Smets N, Van Damme S, De Wilde D, Weyns G, Deconinck J (2007) J Appl Electrochem 37(11):1345
14. Van Damme S, Nelissen G, Van Den Bossche B, Deconinck J (2006) J Appl Electrochem 36(1):1
15. Nelissen G, Van Den Bossche B, Deconinck J, Van Theemsche A, Dan C (2003) J Appl Electrochem 33(10):863
16. Newman J (1991) Electrochemical systems. Prentice Hall, Englewood Cliffs
17. Nelissen G (2003) Simulation of multi-ion transport in turbulent flow. Dissertation, Vrije Universiteit Brussel, Brussels
18. Nelissen G, Van Theemsche A, Dan C, Van Den Bossche B, Deconinck J (2004) J Electroanal Chem 563(2):213
19. Waterson N (2003) Simulation of turbulent flow heat and mass transfer using a residual-distribution approach. Dissertation, Technical University Delft, Delft
20. Dan C, Van Den Bossche B, Bortels L, Nelissen G, Deconinck J (2001) J Electroanal Chem 505:12
21. Purcar M (2005) Development and evaluation of numerical models and methods for electrochemical machining and electroforming applications. Dissertation, Vrije Universiteit Brussel, Brussels
22. Altena H (2000) Precision ECM by process characteristic modelling. Dissertation, Glasgow Caledonian University, Glasgow
23. Schenk O, Gaertner K (2004) J Future Gener Comput Syst 20(3):475
24. Schenk O, Gaertner K (2006) Elec Trans Numer Anal 23:158